

# Shell closure at $N = 34$ and the $^{48}\text{Si}$ nucleus

G. Co<sup>1,2</sup>, M. Anguiano<sup>3</sup>, A. M. Lallena<sup>3</sup>

<sup>1</sup> *Dipartimento di Matematica e Fisica "E. De Giorgi",  
Università del Salento, I-73100 Lecce, Italy*

<sup>2</sup> *INFN Sezione di Lecce,  
Via Arnesano, I-73100 Lecce, Italy*

<sup>3</sup> *Departamento de Física Atómica,  
Molecular y Nuclear, Universidad de Granada,  
E-18071 Granada, Spain*

(Dated: September 23, 2019)

By using a non-relativistic independent particle model we investigate the mechanism promoting 34 as new magic number. We carried out Hartree-Fock plus Bardeen-Cooper-Schrieffer and Quasi-particle Random Phase Approximation calculations by consistently using the same finite-range interaction in all the three steps of our approach. We used four Gogny-like interactions, with and without tensor terms. We find that the shell closure for  $N = 34$  neutrons appears in isotones with  $Z < 26$  protons. The smaller is the proton number, the more evident is the shell closure at  $N = 34$ . An ideal nucleus to investigate this effect should be  $^{48}\text{Si}$ , as it has been recently suggested. However, some discrepancies occur between the results obtained with the four effective interactions we used concerning the position of the two-neutron drip line and, therefore, the existence of  $^{48}\text{Si}$ . The experimental identification of this nucleus could shed light about the shell evolution in nuclei far from the stability valley and put stringent tests on nuclear structure theories.

PACS numbers: 21.10.-k, 21.10.Dr, 21.10.Pc, 21.60.-n, 21.60.Cs

The existence of magic numbers is the main phenomenological evidence justifying the application of an independent particle model (IPM) to describe atomic nuclei. In this approach, the many-body states are Slater determinants of single particle (s.p.) states. The s.p. properties, such as energy or angular momentum, are meaningful in this model, even though the measured quantities are only those of the global nuclear system.

The nuclear ground state in the IPM model is built by considering that all the s.p. levels below the Fermi energy are occupied in accordance with the Pauli exclusion principle. In spherical systems, a s.p. state with angular momentum  $j$  presents a  $2j + 1$  degeneracy. The magic numbers appear when the occupancy of all the s.p. levels below the Fermi energy is at its maximum. The energy ordering of the s.p. states selects the values of the magic numbers, which in the surroundings of the stability valley show the well known sequence: 2, 8, 20, 28, 40, 50, 82, 126.

The observation that these magic numbers are not the same in all the regions of the nuclear chart, but change when going far away from the stability valley has been a surprise (see for example the reviews of Gade and Glasmacher [1] and Sorlin and Porquet [2] for a survey). One of the predicted new magic numbers is 34, whose occurrence is due to a subtle interplay between spin-orbit and tensor terms of the nuclear interaction [3].

Several authors have investigated, both theoretically and experimentally, the appearance of the  $N = 34$  closure in Ca and Ti isotopes [4–11]. However, while this shell closure seems to be well established in  $^{54}\text{Ca}$ , no clear conclusions have been drawn in the case of  $^{56}\text{Ti}$ .

Recently, it has been argued that a more clear signature of the emergence of this new magic number would be provided by the existence of the neutron rich nucleus  $^{48}\text{Si}$  [12]. This prediction has been formulated by using relativistic IPM calculations.

The magic number 34 appears in the  $pf$ -shell if the energy of the  $2p_{1/2}$  s.p. state is smaller than that of the  $1f_{5/2}$  level and the energy gap between them is significant. In this manner, the occupation of the former state and the emptiness of the latter one build up a shell closure at 34.

The occurrence of this situation relies on the subtle combination of different effects. Let us assume, for example, that the mean field potential where the nucleons move independently of each other is a Woods-Saxon well [13]:

$$U(r) = -V_0 f(r) + V_{\text{is}} \frac{r_0^2}{r} \frac{df(r)}{dr} \mathbf{l} \cdot \mathbf{s}, \quad (1)$$

where

$$f(r) = \frac{1}{1 + \exp[(r - R)/a]} \quad (2)$$

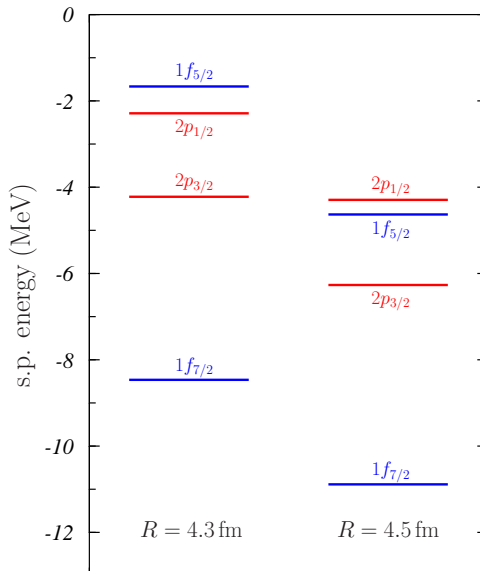


Figure 1: Energies of the s.p. levels  $2p$  and  $1f$  obtained with the Woods-Saxon potential, defined in eq. (1). Results for two values of  $R$  are shown.

and  $\mathbf{l}$  and  $\mathbf{s}$  are, respectively, the s.p. orbital angular momentum and spin operators. We consider the case with  $V_0 = 50$  MeV,  $V_{\text{is}} = 9$  MeV,  $r_0 = 1.25$  fm,  $a = 0.53$  fm and  $R = 4.3$  fm. The energies of the two levels of interest are those shown in the left column of fig. 1, and in this case we obtain the level ordering generating the  $N = 34$  shell closure.

If we change  $R$  from 4.3 fm to 4.5 fm the  $1f$  and  $2p$  levels are pushed down but their energy difference increases, the  $2p_{1/2}$  level lies above the  $1f_{5/2}$ , and therefore we do not have any more a shell closure at  $N = 34$  (see the right column of fig. 1).

In this work we present the results that we have obtained by investigating the emergence of this new magic number by using a non-relativistic IPM approach which uses a Hartree-Fock (HF) plus Bardeen-Cooper-Schrieffer (BCS) model for the ground states, and a Quasi-particle Random Phase Approximation (QRPA) for the description of the excited states. The sets of s.p. wave functions have been generated by carrying out (HF) calculations with density dependent finite-range interactions of Gogny type. We used these results as input of a BCS calculation in order to take into account the effects of the pairing. In refs. [14–16] we have shown the good agreement between the results of our HF+BCS approach with those of Hartree-Fock-Bogoliubov (HFB) calculations.

The HF s.p. wave functions and the BCS output, in terms of changes of the HF s.p. energies and modifications of the occupation numbers of the HF s.p. levels, have been used in QRPA calculations in order to obtain the excitation energies of the  $2^+$  states. A detailed description of the QRPA formalism is given in the work by De Donno et al. [17].

We consistently use the same finite-range interaction in all the three steps of our calculations. Specifically, we have carried out the present investigation by using four different parameterizations of the density-dependent finite-range Gogny interaction. These parameterizations are those known in the literature as D1S [18], D1M [19], D1ST2a [20] and D1MTd [21]. The parameters of the first two forces were selected, with a procedure described in detail by Chappert [22], by fitting binding energies, root mean square (rms) charge radii and fission properties of a wide set of nuclei. In the present context it is relevant to remark that the strength of the spin-orbit term of the interaction was adjusted to reproduce the experimental energy splitting between the  $1p_{1/2}$  and  $1p_{3/2}$  neutron s.p. levels in  $^{16}\text{O}$ .

The other two forces, D1ST2a and D1MTd have been constructed by adding to the D1S and D1M interactions, respectively, one isospin dependent and one isospin independent tensor components. These tensor terms modify sensitively the splitting of the s.p. spin-orbit partner levels [23], but do not affect most of the quantities considered in the force fitting above mentioned. The strengths of the spin-orbit and tensor terms of the D1MTd force were chosen to properly describe the excitation energies of the low-lying  $0^-$  states in  $^{16}\text{O}$  and in  $^{48}\text{Ca}$  [21], while those of the D1ST2a were selected to reproduce the excitation energy of the  $0^-$  states in  $^{16}\text{O}$  and the energy splitting between the  $1f$  s.p. states in  $^{48}\text{Ca}$  [20].

By using the approach described above, we investigated the region of the nuclear chart where changes in the ordering of the  $1f_{5/2}$  and  $2p_{1/2}$  levels may occur. Specifically, we have calculated the evolution of the s.p. energies of these two levels for the sequence of  $N = 34$  isotones from  $^{48}\text{Si}$  to  $^{66}\text{Ge}$ .

All these nuclei have been considered to be spherical. While this permits a rather good description of the slightly deformed  $^{58}\text{Cr}$ ,  $^{60}\text{Fe}$  and  $^{62}\text{Ni}$  nuclei, it turns out to be a rather poor approximation for the more heavily deformed  $^{64}\text{Zn}$  and  $^{66}\text{Ge}$  nuclei. The agreement with the available experimental data is, however, rather satisfactory. Our calculations slightly underbind the nuclei investigated but the largest relative difference with the experimental binding energy is of about 1.3%. It is not a surprise that this is the value we found for the two most deformed nuclei quoted above.

We show in the panels (a) and (c) of fig. 2 the s.p. energies  $\epsilon_k$  of the  $1f_{5/2}$  and  $2p_{1/2}$  levels, obtained in our HF calculations by using the D1ST2a and D1MTd interactions presented above, for the aforementioned set of  $N = 34$  even-even isotones. For comparison, in the panels (b) and (d) of the same figure, we show the pairing corrected HF+BCS quasi-particle energies defined as

$$\epsilon_k^{\text{HF+BCS}} = \begin{cases} \lambda - E_k^q, & \text{if } \epsilon_k < \lambda, \\ \lambda + E_k^q, & \text{if } \epsilon_k > \lambda, \end{cases} \quad (3)$$

where  $\lambda$  is the chemical potential obtained in the BCS calculation and  $E_k^q$  is the corresponding quasi-particle energy. Similar results are obtained with the D1S and D1M interactions.

As seen in fig. 2, the various calculations predict that in the nuclei with  $Z < 26$  the s.p. energy of the  $2p_{1/2}$  level (red open squares) is lower than that of the  $1f_{5/2}$  level (blue solid circles).

This behavior is rather general, and is related to the increase of the radial dimensions of the neutron effective potential generated by HF calculations when the proton number increases. We tested this fact by carrying out HF calculations with the Skyrme SkI interaction for a fixed number of neutrons and by increasing the proton numbers. We observed a growth of the radial dimensions of the effective potential and, for the s.p. energies, we obtained the same effect shown in fig. 1 for a simple Woods-Saxon potential. We can state that the observed trend is an overall effect of the nuclear mean field with small differences among the different effective nuclear interactions considered.

These results indicate that the best nuclei to identify the emergence of the new magic number 34 are those with the smallest proton number  $Z$  where the energy difference between the  $1f_{5/2}$  and the  $2p_{1/2}$  states is accentuated. This makes the  $^{48}\text{Si}$  nucleus a good testing ground for these studies, as pointed out by Li et al. [12].

We investigated the peculiar properties of this nucleus by considering how pairing effects evolves in the silicon isotope chain. We considered only even-even nuclei from  $^{32}\text{Si}$  up to  $^{48}\text{Si}$  and assumed a spherical shape for all these isotopes. While the deformations of  $^{40}\text{Si}$  and  $^{44}\text{Si}$  are relatively small, those of  $^{42}\text{Si}$  and  $^{44}\text{Si}$  are instead remarkable [24].

We show in table I the total HF+BCS binding energies of the Si isotopes under investigation obtained with the four interactions we have considered. In the cases of D1S and D1M interactions the binding energy of  $^{48}\text{Si}$  is slightly smaller than that of  $^{46}\text{Si}$  nucleus. This indicates that, for these two forces,  $^{48}\text{Si}$  is beyond the two-neutron drip line.

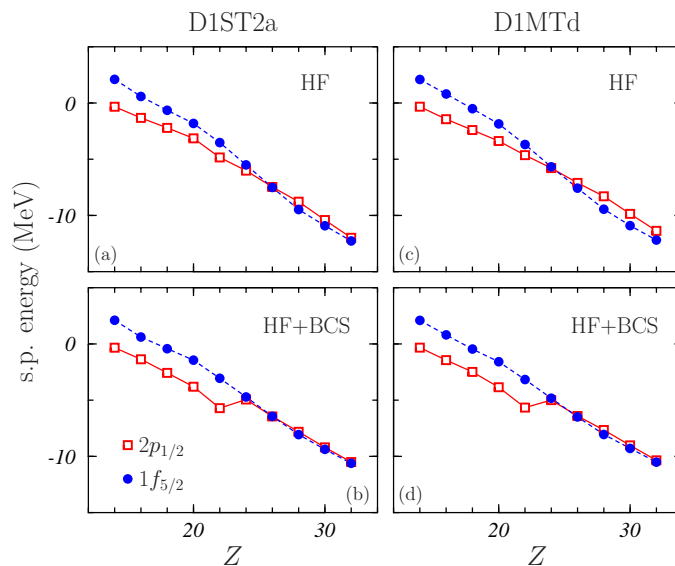


Figure 2: Energies of the  $1f_{5/2}$  (blue solid circles) and of the  $2p_{1/2}$  (red open squares) calculated in HF (panels (a) and (c)) and in HF+BCS (panels (b) and (d)) with the D1ST2a (panels (a) and (b)) and the D1MTd (panels (c) and (d)) interactions for a sequence of  $N = 34$  isotones from the  $^{48}\text{Si}$  to the  $^{66}\text{Ge}$ .

$N$	$A$	D1S	D1ST2a	D1M	D1MTd	exp
18	32	-268.8	-265.6	-265.1	-264.8	-271.4
20	34	-282.3	-283.2	-279.9	-282.3	-283.4
22	36	-288.9	-287.3	-285.9	-286.7	-292.1
24	38	-296.1	-292.8	-292.8	-292.5	-299.9
26	40	-302.4	-297.6	-299.2	-297.6	-306.5
28	42	-307.7	-302.2	-304.6	-302.0	-311.6
30	44	-309.8	-304.4	-306.7	-304.4	-315.7
32	46	-311.5	-305.7	-308.7	-306.5	
34	48	-311.2	-305.7	-308.5	-306.7	

Table I: Total HF+BCS binding energies, in MeV, of the Si isotopes under investigation. The experimental values are taken from the Brookhaven National Lab compilation [25].

The situation is reversed for the D1MTd interaction, while for the D1ST2a force both nuclei have the same binding energy.

By changing of 10% the numerical input parameters, such as integration range and number of integration points in both radial and momentum space, we estimated the numerical uncertainty of our calculations. In the case of the binding energies it resulted of about 0.3% and then the small differences obtained between the total binding energies are within our numerical accuracy.

The results of table I indicate that, in our model, the  $^{48}\text{Si}$  nucleus is at the edge of the two-neutron emission drip line. The HFB results of the Amedee database [24], obtained with the Gogny D1S force, places  $^{48}\text{Si}$  beyond the drip line. On the other hand, the results presented in the supplementary information of the work by Erler et al. [26], obtained with various parameterizations of the Skyrme interaction, indicate that the  $^{48}\text{Si}$  nucleus is positioned before the drip line for all the forces considered but for SLy4. The results of HFB calculations we carried out with the HFBRAD code [27] indicate that also the SIII force predicts a  $^{48}\text{Si}$  nucleus beyond the drip line. The recent compilation of relativistic HFB results of Xia et al. [28] finds  $^{48}\text{Si}$  before the two-neutron drip line. Then, the position of the drip line in Si isotopes is an open problem from the theoretical point of view.

We continued our investigation by considering henceforth only the two interactions containing tensor terms, D1ST2a and D1MTd, which generate a  $^{48}\text{Si}$  stable against the two-nucleon emission.

One of the key features of the magic numbers is the absence, or the strong reduction, of pairing effects. For the set of silicon isotopes that we investigated, we collect in table the values of some quantities indicative of the relevance of the pairing. With  $\Delta N^2$  we indicate the fluctuation of the particle number in BCS calculations. The rows labelled as  $B_p/A$  show the contribution of the pairing to the nuclear binding energy per nucleon, expressed in MeV. Finally,

$$\Delta r = \frac{|r^{\text{HF+BCS}} - r^{\text{HF}}|}{r^{\text{HF}}} \quad (4)$$

$N$	$A$	D1ST2a			D1MTd		
		$\Delta N^2$	$-B_p/A$ (MeV)	$\Delta r$ (%)	$\Delta N^2$	$-B_p/A$ (MeV)	$\Delta r$ (%)
18	32	2.66	0.11	$2 \cdot 10^{-3}$	2.62	0.10	$2 \cdot 10^{-3}$
20	34	$4 \cdot 10^{-4}$	$3 \cdot 10^{-4}$	$1 \cdot 10^{-6}$	$1 \cdot 10^{-4}$	$2 \cdot 10^{-4}$	$7 \cdot 10^{-7}$
22	36	3.24	0.09	$4 \cdot 10^{-3}$	3.22	0.08	$3 \cdot 10^{-3}$
24	38	4.36	0.12	$6 \cdot 10^{-3}$	4.29	0.10	$4 \cdot 10^{-3}$
26	40	3.41	0.11	$5 \cdot 10^{-3}$	3.32	0.08	$4 \cdot 10^{-3}$
28	42	0.25	0.09	$2 \cdot 10^{-3}$	0.04	0.04	$3 \cdot 10^{-4}$
30	44	2.39	0.12	$4 \cdot 10^{-3}$	2.24	0.07	$2 \cdot 10^{-3}$
32	46	$6 \cdot 10^{-4}$	0.10	$8 \cdot 10^{-6}$	$8 \cdot 10^{-4}$	0.07	$2 \cdot 10^{-6}$
34	48	$7 \cdot 10^{-4}$	0.10	$2 \cdot 10^{-5}$	$5 \cdot 10^{-5}$	0.07	$7 \cdot 10^{-7}$

Table II: Some quantities related to pairing effects calculated for the silicon isotope chain. Each nucleus is here identified by the neutron and mass numbers,  $N$  and  $A$ , respectively. The quantity  $\Delta N^2$  indicates the fluctuation of the number of particles. The pairing energy,  $B_p/A$ , is the contribution of the pairing to the total nuclear binding energy per nucleon. Finally,  $\Delta r$ , defined in eq. (4), gives the relative difference between the neutron rms radii obtained in HF+BCS and HF calculations.

gives the relative difference between the rms radii calculated in HF+BCS and in HF calculations.

All the three quantities under investigation show analogous behaviors for both interactions. The smallest values, indicating small pairing effects, appear for  $N = 20$ , corresponding to the closure of the  $1d_{3/2}$  level, and for  $N = 28$ , due to the complete occupancy of the  $1f_{7/2}$  s.p. state. The values of the three quantities increase for the nucleus  $^{44}\text{Si}$  where the  $2p_{3/2}$  level is only half filled. The full occupancy of this level strongly reduces the pairing effects for  $N = 32$  and indicates a shell closure that has been already investigated in Ca and Ti isotopes [4–11]. A similar situation occurs for  $N = 34$  where the  $2p_{1/2}$  is completely filled and the extremely low values of  $\Delta N^2$  and  $\Delta r$  point to it as a magic number.

The isotopic evolution of the first  $2^+$  excited state may also indicate a shell closure [1, 2]. We have calculated the  $2^+$  excited states of various Si isotopes by using the QRPA. In this approach, the nuclear excited states are described as linear combinations of one-particle one-hole, one-particle one-particle, or one-hole one-hole configurations. More complicated configurations, such as  $n$ -particle  $n$ -hole or  $n$ -particle  $n$ -particle configurations, are neglected.

The QRPA results are very sensitive to the dimensions of the s.p. configuration space. We have selected its size to avoid imaginary energy solutions and to reproduce at best the behavior of the known experimental energies, i.e. those of the  $^{40}\text{Si}$  and  $^{42}\text{Si}$  nuclei.

Following these criteria, we selected all the particle-hole configurations with excitation energy differences smaller than 30 MeV and the particle-particle pairs with maximum excitation energy of 10 MeV. In addition, we did not consider those particle-particle pairs where the product of their occupation numbers is smaller than  $10^{-4}$ . This last restriction reduces noticeably the particle-particle configuration space but it changes the energies of the first  $2^+$  excited states by less than 1%.

We show in table the excitation energies,  $\omega$ , and the  $B(E2)$  values of the first  $2^+$  excited state of the even-even Si isotopes from  $A = 40$  up to  $A = 48$ , obtained with the D1ST2a and D1MTd interactions, as well as the two known experimental excitation energies. The energy difference between these two energies is well reproduced by our calculations, even though the values that we have obtained are shifted by  $\sim 0.5$  MeV. This may be due to the fact that both  $^{40}\text{Si}$  and  $^{42}\text{Si}$  are deformed nuclei [24].

The largest excitation energy of the  $2^+$  states shown in table is that of the  $N = 34$  isotope. This occurs for both the interactions considered and it can be considered as an additional hint of the  $N = 34$  shell closure.

In conclusion, we have investigated the emergence of a new magic number at  $N = 34$ . For nuclei far from the stability valley with low  $Z$ , the corresponding shell closure occurs because the energy of the s.p.  $2p_{1/2}$  state is smaller than that of the  $1f_{5/2}$  level up to  $Z \sim 24$  where the ordering of these two s.p. states is reversed. Even more, the lower the  $Z$  value is, the larger becomes the energy gap, thus favoring the appearance of the new magic number. This effect is related to the radial dimension of the neutron effective potential that increases with  $Z$  along the  $N = 34$  isotonic chain.

Our non-relativistic calculations confirm the findings of Li et al. [12] indicating the  $^{48}\text{Si}$  nucleus as a good candidate to identify the shell closure at  $N = 34$ . However, it is worth pointing out that this nucleus is very close to the two-neutron emission drip line. For example, our results for the D1S and D1M forces indicate that the  $^{48}\text{Si}$  is beyond this line, while the two interactions with tensor terms, D1ST2a and D1MTd, situate it before the drip line.

In any case, it must to be noted that, although the results seem discrepant, the differences between them are within the limit of the numerical accuracy of our calculations. In these circumstances we believe that to elucidate experimentally the positioning of the drip line in Si isotopes and the eventual existence of the  $^{48}\text{Si}$  nucleus would be a challenging investigation that could shed light on the behavior of the shell evolution far from the stability valley, and set stringent limits to the nuclear theories.

		D1ST2a		D1MTd		experiment
		$\omega$	$B(E2)$	$\omega$	$B(E2)$	$\omega$
$N$	$A$	(MeV)	( $e^2 \text{ fm}^4$ )	(MeV)	( $e^2 \text{ fm}^4$ )	(MeV)
26	40	1.45	81.9	1.49	84.7	0.986
28	42	1.24	37.5	1.28	2.4	0.77
30	44	0.45	186.2	0.52	101.5	
32	46	1.24	70.4	1.10	65.3	
34	48	1.61	30.1	1.61	24.7	

Table III: QRPA results for the excitation of the first  $2^+$  state in some Si isotopes calculated by using the D1ST2a and the D1MTd interactions. We have indicated with  $\omega$  the excitation energy. The experimental values quoted for the  $^{40}\text{Si}$  and  $^{42}\text{Si}$  isotopes are from Campbell et al. [29] and Bastin et al. [30], respectively.

### Acknowledgments

This work has been partially supported by the Junta de Andalucía (FQM387), the Spanish Ministerio de Economía y Competitividad (FPA2015-67694-P) and the European Regional Development Fund (ERDF).

- 
- [1] A. Gade, T. Glasmacher, *Prog. Part. Nucl. Phys.* **60**, 161 (2008).
  - [2] O. Sorlin, M.-G. Porquet, *Prog. Part. Nucl. Phys.* **61**, 602 (2008).
  - [3] M. Grasso, *Phys. Rev. C* **89**, 034316 (2014).
  - [4] R. V. F. Janssens, et al., *Phys. Lett. B* **546**, 55 (2002).
  - [5] S. N. Liddick, et al., *Phys. Rev. C* **70**, 064303 (2004).
  - [6] B. Fornal, et al., *Phys. Rev. C* **70**, 064304 (2004).
  - [7] B. Fornal, et al., *Phys. Rev. C* **72**, 044315 (2005).
  - [8] M. Honma, et al., *Eur. Phys. Jour. A* **25 (S1)**, 499 (2005).
  - [9] F. Wienholtz, et al., *Nature* **498**, 346 (2013).
  - [10] D. Steppenbeck, et al., *Nature* **502**, 207 (2013).
  - [11] S. N. Liddick, et al., *Phys. Rev. Lett.* **92**, 072502 (2004).
  - [12] J. J. Li, et al., *Phys. Lett. B* **788**, 192 (2019).
  - [13] A. Bohr, B. R. Mottelson, *Nuclear structure, vol. I* (Benjamin, New York, 1969).
  - [14] M. Anguiano, et al., *Nucl. Phys. A* **955**, 181 (2016).
  - [15] M. Anguiano, et al., *Eur. Phys. Jour. A* **52**, 183 (2016).
  - [16] M. Anguiano, et al., *Phys. Rev. C* **99**, 034302 (2019).
  - [17] V. De Donno, et al., *Phys. Rev. C* **95**, 054329 (2017).
  - [18] J. F. Berger, M. Girod, D. Gogny, *Comp. Phys. Commun.* **63**, 365 (1991).
  - [19] S. Goriely, et al., *Phys. Rev. Lett.* **102**, 242501 (2009).
  - [20] M. Grasso, M. Anguiano, *Phys. Rev. C* **88**, 054328 (2013).
  - [21] G. Co', et al., *Phys. Rev. C* **97**, 034313 (2018).
  - [22] F. Chappert. Ph.D. thesis, Nouvelles paramétrisation de l'interaction nucléaire effective de Gogny, Université de Paris-Sud XI, 2007; available at:  
<http://tel.archives-ouvertes.fr/tel-001777379/en/>.
  - [23] T. Otsuka, T. Matsuo, D. Abe, *Phys. Rev. Lett.* **97**, 162501 (2006).
  - [24] S. Hilaire, M. Girod, *Hartree-Fock-Bogoliubov results based on the Gogny force. Amedee database*, [http://www-phynu.cea.fr/HFB-Gogny\\_eng.htm](http://www-phynu.cea.fr/HFB-Gogny_eng.htm).
  - [25] Brookhaven National Laboratory, *National Nuclear Data Center*,  
<http://www.nndc.bnl.gov/>.
  - [26] J. Erler, et al., *Nature* **486**, 509 (2012).
  - [27] K. Bennaceur, J. Dobaczewski, *Comput. Phys. Comm.* **168**, 96 (2005).
  - [28] X. W. Xia, et al., *At. Data Nucl. Data Tables* **121-122**, 1 (2018).
  - [29] C. M. Campbell, et al., *Phys. Rev. Lett.* **97**, 112501 (2006).
  - [30] B. Bastin, et al., *Phys. Rev. Lett.* **99**, 022503 (2007).